



HAL
open science

Inertia-driven jetting regimes in microfluidic coflows

Fan Zhang, Arnaud Erriguible, Théo Gavaille, Mike T. Timko, Samuel Marre

► **To cite this version:**

Fan Zhang, Arnaud Erriguible, Théo Gavaille, Mike T. Timko, Samuel Marre. Inertia-driven jetting regimes in microfluidic coflows. *Physical Review Fluids*, 2018, 9 (3), 092201(R) (9 p.). 10.1103/PhysRevFluids.3.092201 . hal-01866650

HAL Id: hal-01866650

<https://hal.science/hal-01866650v1>

Submitted on 3 Sep 2018

HAL is a multi-disciplinary open access archive for the deposit and dissemination of scientific research documents, whether they are published or not. The documents may come from teaching and research institutions in France or abroad, or from public or private research centers.

L'archive ouverte pluridisciplinaire **HAL**, est destinée au dépôt et à la diffusion de documents scientifiques de niveau recherche, publiés ou non, émanant des établissements d'enseignement et de recherche français ou étrangers, des laboratoires publics ou privés.

Inertia-Driven Jetting Regimes in Microfluidic Coflows

Fan Zhang,¹ Arnaud Erriguible,^{1,2,*} Théo Gavaille,^{1,3} Mike T. Timko,⁴ and Samuel Marre^{1,†}

¹*CNRS, Univ. Bordeaux, Bordeaux INP, ICMCB, UMR 5026, F-33600, Pessac, France*

²*CNRS, Univ. Bordeaux, I2M, UMR 5295, F-33600, Pessac, France*

³*IFPEN, 1 & 4, Avenue de Bois-Préau 92852 Rueil-Malmaison, France*

⁴*Department of Chemical Engineering - Worcester Polytechnic Institute, 100 Institute road, Worcester, MA 01609, USA*

(Dated: September 3, 2018)

Microfluidics have been used extensively for study of flows of immiscible fluids, with specific focus on the effects of interfacial forces on flow behavior. In comparison, inertia-driven flow of confined coflowing fluids has received scant attention at the microscale, despite the fact that the effects of microscale confinement are expected to influence inertia-driven flow behavior as observed in free jets. Herein, we report three distinct modes for break-up of co-flowing, confined, microscale jets: the conventional Rayleigh mode and two additional inertia-driven modes occurring at higher Reynolds numbers flows, namely a sinuous wave breakup and an atomization-like mode. Each of the three modes is differentiated by a characteristic droplet size, size distribution, and dependence of the jet length as a function of the external fluid velocity (v_{ext}). A unified phase diagram is proposed to categorize the jet breakup mechanisms and their transitions using as a scaling factor the ratio of the jet inertial forces to the sum of the viscous and interfacial forces for both the inner and outer fluids. These results provide fundamental new insight into the flow behavior of microscale-confined co-flowing jets.

Droplets and jets are of primary importance for applications such as generation of emulsions with at sub-micron scale objects, sprays, and other multiphase flows, all of which are involved in a wide variety of chemical and industrial processes. Multiphase flows have been especially useful to the microfluidics community since dripping and jetting can be used to generate nearly monodisperse droplets that act as nanoliter reactors in series to ensure precise control of residence time and residence time distributions, with enhancing mixing [1]. Such approaches have been extensively used for microfluidics applications including foams generation [2–4], droplets-based microfluidic [5], jet stabilization [6, 7], organic and inorganic micro and nanostructures synthesis [8], and chemical reactions [9, 10].

Jets are metastable hydrodynamic structures, which eventually break into droplets. Jet breakup is a well-known behavior, which occurs via various mechanisms, depending on the properties (velocity, density, viscosity, surface tension, etc.) of the fluid forming the jets and of the outer fluid [11]. Coflow geometries have been considered extensively to study the dripping-to-jetting transition in confined geometries, both for liquid-liquid and liquid-gas coflows [12–15]. This transition depends on the propagation of an absolute instability originating from a growing disturbance downstream, itself arising from the Rayleigh–Plateau instability [16].

Several works report detailed comprehensive modeling of the dripping-to-jetting transition observed in liquid-liquid and liquid-gas microsystems [13, 17–19] for low Reynolds numbers flows ($Re \equiv (v\rho d)/\eta$), typically $Re < 10$, where ρ is the fluid density, v is the fluid velocity, d is the flow characteristic length and η is the dynamic viscosity. In such cases, the dripping and Rayleigh jetting regimes and the transitional boundaries between them

can be organized using a map of the inner fluid Weber number ($We_{in} \equiv (v_{int}^2 \rho_{int} d)/\sigma$), where σ is the interfacial tension between the two immiscible fluids, versus outer fluid Capillary number ($Ca_{ext} \equiv (v_{ext} \eta_{ext})/\sigma$), as previously described [13, 14].

Aside from the Rayleigh regime observed for confined flows, jets exhibit other breakup modes that have been investigated for jetting into quiescent outer fluids [20]. Four distinct jetting regimes have been identified and reported so far [21] including the Rayleigh mode, the first and second wind induced breakup modes, and the atomization regime [22, 23]. These regimes and the transitions between them depend on several factors such as inertia, interfacial tension, and viscosity ratio of the fluids [24].

Even though inertia-driven jet breakup regimes occurring at larger Reynolds numbers ($Re > 100$) have been identified and detailed in several experimental works of unconfined jets, the case of microscale confined jetting has received scant attention. This is primarily due to the technical difficulties encountered when studying the high flowrates required to reach high Re regimes and the resulting high pressure drops, which complicate experimental investigation.

Studies using high pressure microsystems can access high Re regimes consisting of gas-liquid, liquid-liquid, and even supercritical fluid (SCF)-liquid components. Recent publications have demonstrated the use of microfluidic systems at high pressures [26–28]. SCFs are of particular interest as working fluids, as they combine liquid-like densities and gas-like viscosities [25]. Moreover, SCFs properties can be adjusted with minor changes of pressure and/or temperature, permitting study of inertial-viscous regimes that might otherwise be difficult to access experimentally. Accordingly, the use of high-pressure microsystems and SCFs permits the study of

new conditions of flow fragmentation that have not been investigated previously. Of particular interest are inertia-driven regimes, where inertial forces ($F_{iner} = \rho v^2 d^2$) can overcome viscous ($F_v = \eta v d$) and interfacial ($F_{ITF} = \sigma d$) forces that typically dominate at the microscale. Previous work has exploited the experimental flexibility afforded by SCFs, and dripping to jetting transition has already been reported for a micro-confined liquid/SCFs co-current flow [29, 34]. In this letter, we identify three jetting modes observed for co-flows of either dense CO_2 (liquid or supercritical) or liquid pentane and water in a capillary microreactor. Each mode was identified by distinctive droplet sizes, size distributions, and the evolution of the jet length and shape. These are the first reported observations of such modes under microscale confined conditions.

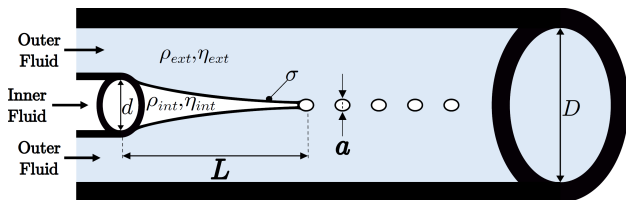


Figure 1. Coflowing set-up developed for this study. D and d are the inner diameters of the outer and inner tubing, respectively. L is the jet length, while a is the droplets diameter.

The experimental high pressure set-up is composed of two silica capillaries inserted within one another (outer capillary: $D = 247 \pm 6 \mu\text{m}$ and inner capillary $d_{ext} = 167 \pm 6 \mu\text{m}$ and $d = 100 \pm 3 \mu\text{m}$), as shown in Fig.1. Accordingly, the external hydraulic diameter D_h of the outer fluid is defined as: $D_h = (D^2 - d_{ext}^2) / d_{ext}^2$. Two high pressure syringe pumps (Teledyne ISCO 100DM) were used to feed CO_2 or pentane and water at constant flow rates, while a third pump was used in constant pressure mode as a back pressure regulator to maintain constant the outlet pressure at $p = 10 \text{ MPa}$ for the CO_2 -water system, *i.e.* above the critical pressure of CO_2 ($p_c(CO_2) = 7.38 \text{ MPa}$) or at $p = 0.1 \text{ MPa}$ for the pentane - water system. The capillary assembly was placed in a temperature-controlled bath ($20 < T (^{\circ}\text{C}) < 50$) and the coflow was monitored using a high speed CCD camera (Phantom Miro 340, Vision Research, Inc.) mounted on a binocular microscope. Image resolution was $\sim 1.5 \mu\text{m}/\text{pixel}$, which allowed resolution of features larger than about $5 \mu\text{m}$. Jet lengths, droplets sizes, and size distributions were extracted from still images using the ImageJ software.

Actual fluid velocities inside the microchannel (v_{int} , v_{ext}) were estimated from the pump flow rates and accounting for the temperature dependence of density: $v_i = \frac{Q_i(pump)}{S_i} \times \frac{\rho_i(pump)}{\rho_i(bath)}$, where S_i is the internal cross section area out of which the fluid i is passing, $Q_i(pump)$ is the pump volumetric flowrate, while $\rho_i(pump)$ and $\rho_i(bath)$

Table I. Physical properties and corresponding values for the dimensionless numbers (We , Ca and Re) of CO_2 or pentane and water flows at $p = 10 \text{ MPa}$ (or $p = 0.1 \text{ MPa}$) for $T = 20^{\circ}\text{C}$ (liquid CO_2 and liquid pentane) and $T = 48^{\circ}\text{C}$ (sc- CO_2), respectively.

T P	20 °C 10 MPa		48 °C 10 MPa		20 °C 0.1 MPa
Fluid	Liquid CO ₂	H ₂ O	sc-CO ₂	H ₂ O	Pentan
σ^a (mN m ⁻¹)	37.1	/	28.8	/	51.2
η (μPas)	81.5	998.8	30.6	567.3	227.5
ρ (kg m ⁻³)	856.3	1002.7	421.6	993.2	625.8
We^b	8×10^{-3}	0.01	0.02	0.01	3×10^{-3}
	-	-	-	-	-
Ca^b	1.2	71.9	3.48	91.6	5.5
	1.3×10^{-4}	1.6×10^{-3}	1.3×10^{-4}	1.3×10^{-3}	2.3×10^{-4}
Re^b	-	-	-	-	-
	1.5×10^{-3}	0.15	1.6×10^{-3}	0.11	9.4×10^{-4}
Re^b	62.9	5	159	8.8	14.6
	782.8	463	2217	837	583.7

^a Versus water.

^b Depending on flow rates.

For the calculation, we have used:

$$d = 100 \mu\text{m}, D = 250 \mu\text{m}$$

$$25 < Q_{CO_2} (\mu\text{l}\cdot\text{min}^{-1}) < 1000$$

$$50 < Q_{H_2O} (\mu\text{l}\cdot\text{min}^{-1}) < 10000$$

$$25 < Q_{Pentane} (\mu\text{l}\cdot\text{min}^{-1}) < 1000$$

are the fluid density in the pump (at $p = p_{exp}$ and room temperature - RT) and in the capillary ($p = p_{exp}$ and $T = T_{exp}$), respectively. The physical properties of CO_2 and H_2O at experimental conditions were obtained from the REFPROP software [38] or from the literature [39]. Table I summarizes relevant physical properties and dimensionless numbers used in this work.

The conventional strategy to classify the jet break up regimes is to monitor the evolution of the length of the coherent portion of the jet, the mean droplet size and the droplet size distribution as functions of the external fluid velocity (v_{ext}). In a typical case, four flow regimes can be distinguished (Fig.2).

Dripping. At low flow velocities, the classical dripping regime is observed, displaying an absence of jets with generation of large, monodisperse droplets at the tip of the inner capillary (Fig.2a).

Rayleigh Jetting. With increasing external flow velocity, classical dripping transitions to jetting occur. Jet length grows almost linearly with the external fluid velocity, as shown in Fig.3a. Downstream, the jet eventually breaks into monodisperse droplets due to the Rayleigh-Plateau instability (Fig.2b and 2c and movie [30]). Breakup results from the growth of long wavelength perturbations when the inertial forces ($F_{iner} = \rho v^2 d^2$) become equal to or greater than the interfacial

forces ($F_{ITF} = \sigma d$), *i.e.* $We \sim 1$. These two first regimes, mostly driven by interfacial forces, have been observed and studied several previous times at the microscale for liquid-liquid [13, 14], liquid-gas [19], and supercritical fluid-liquid [29] coflows.

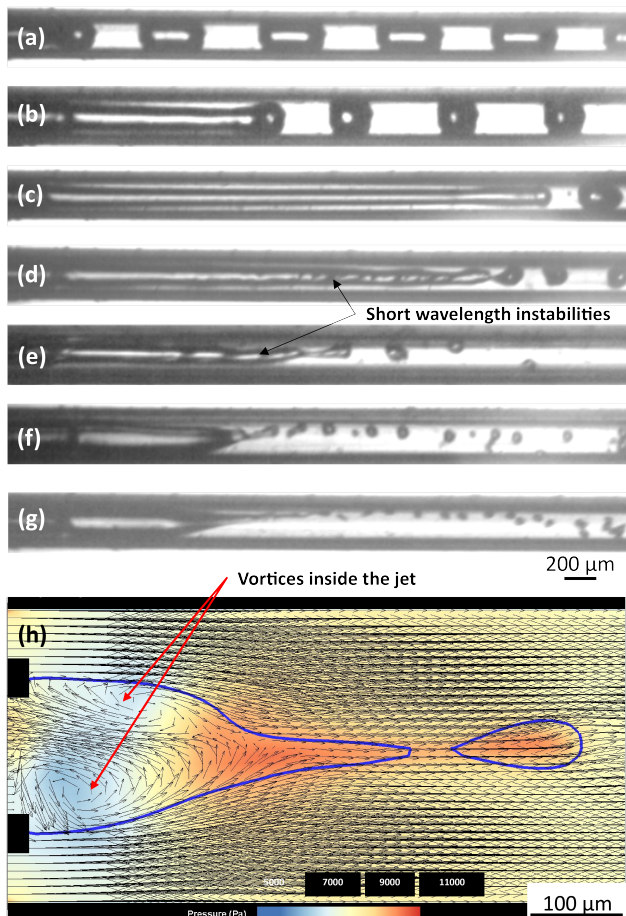


Figure 2. (a) Optical images of the evolution of the jetting as of function of the outer fluid velocity: (a) Dripping, (b, c) Rayleigh jetting, (d, e) Sinuous wave breakup mode, (f, g) atomization-like mode. The pictures were obtained for $p = 10$ MPa, $T = 20^\circ\text{C}$, inner fluid: liquid CO_2 , outer fluid: Water, $v_{int}(\text{CO}_2) = 0.25 \text{ m}\cdot\text{s}^{-1}$, (h) Median plane visualization of the 3D numerical modelling of the atomization-like jetting mechanism displaying the velocity vectors inside the core of the jet ($p = 10$ MPa, $T = 20^\circ\text{C}$, $v_{int}(\text{CO}_2) = 0.25 \text{ m}\cdot\text{s}^{-1}$; $v_{ext}(\text{H}_2\text{O}) = 4 \text{ m}\cdot\text{s}^{-1}$). The arrows represent the velocity vectors, which magnitude are proportional to their length, while the color represents the relative pressure (P_r) spatial variations (the total pressure can be calculated as: $P = P_r + 10 \text{ MPa}$).

Inertia-driven jetting-sinuous wave breakup. With increasing velocity, the jet undergoes destabilization due to the effects of external inertial forces, in contrast with the behavior observed in the Rayleigh jetting mode. The viscous forces ($F_v = \eta v d$), which tend to stabilize the jet, are largely overcome by the inertial forces for $Re > 500$, resulting in the formation of sinuous waves, as previously observed for unconfined flows [22, 24]. In the

sinuous wave breakup regime, breakup stems primarily from the unstable growth of short wavelength perturbations, probably arising from Kelvin-Helmholtz instabilities. The Kelvin-Helmholtz instabilities form due to the localized high velocity ratio (v_{ext}/v_{int}) present on the surface of the jet (Fig.2d and 2e and movie [31]). Two important characteristics can be highlighted: (i) the jet length continuously decreases with increasing outer fluid velocity and, (ii) the polydispersity of the droplet size increases, relative to the distributions observed in the Rayleigh jetting mode, since the jet breaks into fluid ligaments through a pullout mechanism, with the fragments later forming droplets due to Rayleigh mechanism or minimization of surface energy. Filament breaking, which can be described as secondary atomization [40] produces a droplet distribution with much greater polydispersity than is observed in the dripping or Rayleigh jetting regimes (Fig.3b).

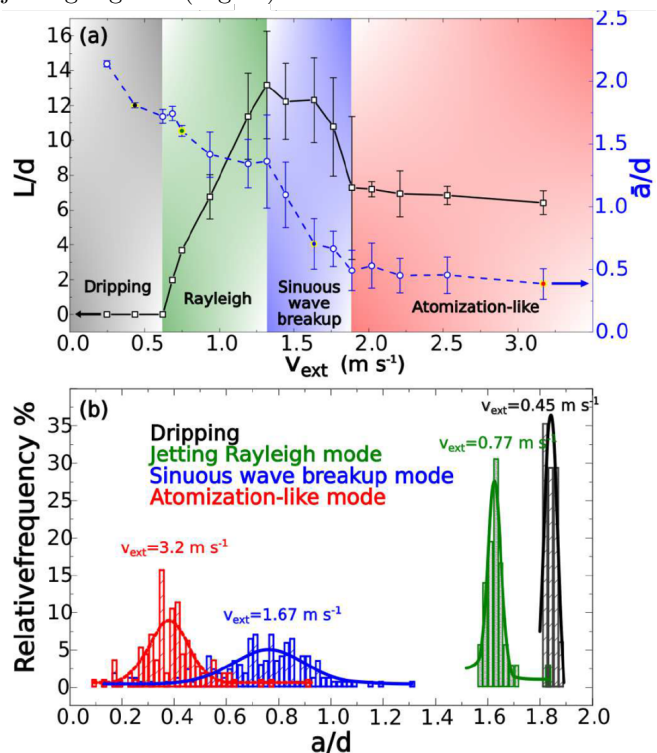


Figure 3. Example of the regimes characteristics used to categorize the breakup mechanisms. (a) Evolution of the jet length and the droplets mean size \bar{a}/d as a function of v_{ext} and (b) the droplets size distributions for different values of v_{ext} , corresponding to yellow circled point in (a). The data were obtained for $p = 10$ MPa, $T = 20^\circ\text{C}$, inner fluid: liquid CO_2 , outer fluid: Water, $v_{int}(\text{CO}_2) = 0.25 \text{ m}\cdot\text{s}^{-1}$.

Inertia-driven jetting-Atomization-like. At high values of external fluid inertial force ($F_{iner,ext}$), the jet length stabilizes with increasing fluid velocity (Fig.2f, Fig.2g and movies [?]). Smaller ligaments form, which transform nearly instantaneously into droplets. In this regime, droplet size can reach values as small as $0.4d$

(Fig.3). One of the main distinguishing features of this regime is characterized by an enlargement of the jet diameter, relative to the nozzle diameter. To confirm this unexpected behavior, we have performed numerical simulations using a 3D incompressible one-fluid model [33], already validated for liquid jet breakup in pressurized CO_2 [34]. This model is selected since the flow behavior is clearly non axisymmetrical for inertial modes (sinuous wave breakup and atomization-like modes). Compressed CO_2 and water used in this work are considered as immiscible fluids in the investigated conditions, so the computational study must account for two-phase flow. Accordingly, the Brackbill model [35] (see ESI) was employed to compute the interfacial forces, while the VOF approach was used with a piecewise linear interface construction (PLIC) for the interface tracking [36]. As observed in numerical simulations (Fig.2h and movies [37]), the high velocity ratio ($v_{ext}/v_{int} > 10$) generates hydrodynamic recirculating vortices within the jet, which confine the inner fluid at the tip and lead to noticeable jet enlargement.

Next, we sought to generalize our observations, by studying the effects of the experimental parameters (inner and outer fluid velocities, p , T) on the interfacial and viscous forces which govern jet behavior. All the three systems (*i.e.* scCO_2 -water, liquid CO_2 -water and pentane - water) were studied so that the widest possible range of experimental parameters could be included in this work and to arrive at the most general possible conclusions. We have varied the experimental parameters to investigate the effects of inertia compared to interfacial and viscous forces. These conditions result in high Reynolds number flows for both the inner and outer fluid (up to $Re = 2200$, Table I), which have not been previously investigated due to the practical restrictions associated with working with high flowrates and the resultant high pressure drops. Investigating these effects provides data to unify in a single picture the four distinct coflow regimes. Utada *et al.* [6] proposed categorizing the transition between the dripping and the jetting regime in micro-coflows using the $[W_{e_{int}}, C_{a_{ext}}]$ diagram, which takes into account the inner flow inertial and interfacial forces, and the outer flow viscous and interfacial forces. These previous studies considered only inner and outer flows with very low inertial forces ($\sim 10^{-3} \mu\text{N}$), possibly preventing observations of the sinuous wave and atomization break up regimes shown here. In contrast, we explored conditions where the inertial forces are in the range $10^{-2} - 10^1 \mu\text{N}$.

We categorize the jetting regimes and their domains of existence by using the ratio of the inertial forces over the sum of the other forces (viscous and interfacial) for both the inner and outer fluid. This approach makes possible the representation of the jet phase diagram, $Y = f(X)$ consisting of a log-log plot non-dimensional scaling parameters: $X = F_{iner,ext}/(F_{TF,ext} + F_{v,ext})$ and $Y = F_{iner,int}/(F_{TF,int} + F_{v,int})$. This non-dimensionalization

emphasizes the effects of inertial forces over viscous and interfacial ones.

In Fig.4, we have represented all available experimental data, and categorized their flow behavior into one of the 4 regimes. Fig.4 provides data for both the sc-CO_2 /water (48°C , 10 MPa), the liquid CO_2 /water (20°C , 10 MPa) and the *liquid* pentane /water (20°C , 0.1 MPa) systems.

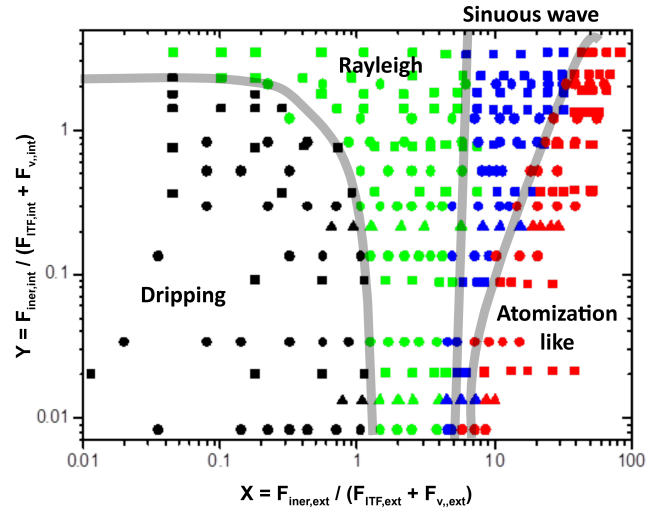


Figure 4. Log-log plot of the ratio (X ; Y) of the inertial forces over the sum of the viscous and interfacial forces for the sc-CO_2 -water ($p = 10$ MPa, $T = 48^\circ\text{C}$: \blacksquare), pentane-water ($p = 0.1$ MPa, $T = 20^\circ\text{C}$: \blacktriangle) and liquid CO_2 - water ($p = 10$ MPa, $T = 20^\circ\text{C}$: \bullet) systems. The dripping regime is indicated in black, the Rayleigh type jets in green, the sinuous wave breakup mode is in blue and the atomization-like mode points are in red.

As a first observation, Fig.4 shows that the transition from dripping to jetting occurs when $X > 1$ and/or $Y > 1$, (Fig.4), as expected. Indeed, the inertial forces at these conditions are greater than the interfacial and viscous forces, leading to jetting.

A remarkable result arises at the transition from Rayleigh jetting to sinuous wave breakup regime. Indeed, the experimental data indicate that, independent of the inner fluid force ratio, the "inertial regime" (*i.e.* sinuous wave and/or atomization-like break up) is never attained provided that $X < 5$ (Fig.4). For $X < 5$, the outer fluid viscous and interfacial forces are sufficient (although smaller than the inertial forces) to stabilize the jet and prevent unstable growth of short wavelength, Kelvin-Helmholtz perturbations that would otherwise lead to the sinuous wave breakup regime. With increasing X , the jet enters the atomization regime. Reaching atomization occurs when the inner fluid viscous and interfacial forces overcome the inertial forces (low Y values, Fig.4). In contrast, when the inertial forces of the inner fluid are sufficient (higher Y values), they tend to extend the length of the jet, stabilizing the sinuous wave break up mode (Fig.4).

The observations and diagram presented in here are not unique to [dense CO_2 (liquid or supercritical) – water] micro coflows. Indeed, the pentane-water system (Fig.4, triangles), obeys the same jetting behavior as the sc- CO_2 - water system (Fig.4, squares) and the liquid CO_2 - water (Fig.4, circles), when non dimensional scaling parameters X and Y are used for data interpretation.

In conclusion, we have studied the jetting behavior of micro-confined co-flows using a high pressure microchannel device. Several fluid-fluid systems were studied, including sc CO_2 - water, liquid CO_2 - water, and pentane - water. In addition to the well know dripping and Rayleigh jetting modes, two new inertia-driven modes were observed, namely the so-called sinuous wave breakup and the atomization-like regime. We find that all our data can be captured by a log-log plot using dimensionless scaling parameters. This study extends previous work on microscale-confined coflowing liquids to permit observation of qualitatively new behavior and unifies previous studies by mapping jet behavior onto a single diagram.

This work provides the basis for many new microfluidics experiments, including those involving production of sub-micron droplets, as reported by other approaches [41]. Future fundamental studies should investigate areas of the phase diagram which remain to be explored, especially those for $Y < 10^{-2}$ and $Y > 10^1$. Data are required at these conditions to provide a full understanding of the transition between between viscous/interfacial-driven flows and inertia driven flows.

This study was supported by the French National Research Agency (ANR SUPERFON), the University of Bordeaux (PhD funding of FZ), The IFPEN (PhD funding of TG), the CNES and the Région Nouvelle Aquitaine. This work has received funding from the European Research Council (ERC) under the European Union’s Horizon 2020 research and innovation program (grant agreement n° 725100, project: Big Mac). MTT thanks the U.S. National Science Foundation for support (CBET 1554283). SM and AE thank Fabien Palencia for technical support.

* erriguible@enscbp.fr

† <http://www.icmcb-bordeaux.cnrs.fr>;
Samuel.Marre@icmcb.cnrs.fr

- [1] R. Seemann, M. Brinkmann, T. Pfohl, S. Herminghaus, Droplet based microfluidics, *Rep. Prog. Phys.*, 75, 016601 (2012).
- [2] R. K. Shah, H. C. Shum, A. C. Rowat, D. Lee, J. J. Agresti, A. S. Utada, L. Y. Chu, J. W. Kim, A. Fernandez-Nieves, C. J. Martinez, and D. A. Weitz, Designer emulsions using microfluidics, *Mater. Today* 11, 18 (2008).
- [3] V. Chokkalingam, S. Herminghaus, R. Seemann, Self-synchronizing pairwise production of monodisperse droplets by microfluidic step emulsification, *Appl. Phys. Lett.* 93, 254101 (2008).
- [4] M. Hashimoto, P. Garstecki, and G. M. Whitesides, Synthesis of Composite Emulsions and Complex Foams with the use of Microfluidic Flow-Focusing Devices, *Small* 3, 1792 (2007).
- [5] S-Y The, R. Lin, L-H Hung, A.P. Lee, Droplet microfluidics, *Lab Chip*, 8, 198 (2008).
- [6] A. S. Utada, L. Y. Chu, A. Fernandez-Nieves, D. R. Link, C. Holtze, and D. A. Weitz, Dripping, Jetting, Drops, and Wetting: The Magic of Microfluidics, *MRS Bull.* 32, 702 (2007).
- [7] T. M. Keenan, C. H. Hsu, and A. Folch, Microfluidic “jets” for generating steady-state gradients of soluble molecules on open surfaces, *Appl. Phys. Lett.* 89, 114103 (2006).
- [8] S. Marre, K.F. Jensen, Synthesis of micro and nanostructures in microfluidic systems, *Chem. Soc. Rev.*, 39, 1183 (2010).
- [9] H. Song, D.L. Chen, R.F. Ismagilov, Reactions in droplets in microfluidic channels, *Angew. Chem. Int. Ed.*, 45(44), 7336 (2006).
- [10] K.S. Elvira, X. Casadevall I solvas, R.C.R. Wootton, A.J. deMello, The past, present and potential for microfluidic reactor technology in chemical synthesis, *Nature Chem.*, 5, 905 (2013).
- [11] Rayleigh, 1879, On the instability of jets, *Proc. Lond. Math. Soc.*, 10, 4-13.
- [12] P. Guillot, A. Colin, A. S. Utada, and A. Ajdari, Stability of a Jet in Confined Pressure-Driven Biphasic Flows at Low Reynolds Numbers, *Phys. Rev. Lett.* 99, 104502 (2007).
- [13] A.A. Utada, A. Fernandez-Nieves, H.A. Stone, D.A. Weitz, Dripping to Jetting Transitions in Coflowing Liquid Streams, *Phys. Rev. Lett.*, 99, 094502 (2007).
- [14] S.Y. Mak, Y. Chao, H.C. Shum, The dripping-to-jetting transition in a co-axial flow of aqueous two-phase systems with low interfacial tension, *RSC Advances*, 7, 3287-3292 (2017).
- [15] C-X. Zhao and A. P. J. Middelberg, Two-phase microfluidic flows, *Chem. Eng. Sci.* 66, 1394 (2011).
- [16] A.S. Utada, A. Fernandez-Nieves, J. M. Gordillo, D.A. Weitz, Absolute Instability of a Liquid Jet in a Coflowing Stream, *Physic. Rev. Lett.*, 100, 014502 (2008).
- [17] M.A. Herrada, A.M. Ganan-Calvo, A. Ojeda-Monge, B. Bluth, P. Riesco-Chueca, Liquid flow focused by a gas: Jetting, dripping, and recirculation, *Phys. Rev. E*, 18(3), 035323 (2008).
- [18] M-L Cordero, F. Gallaire, C.N. Baroud, Quantitative analysis of the dripping and jetting regimes in co-flowing capillary jets, *Phys. Fluids*, 23, 094111 (2011).
- [19] S. Haase, Characterisation of gas-liquid two-phase flow in minichannels with co-flowing fluid injection inside the channel, part I: unified mapping of flow regimes, *Int. J. Multiphase Flows*, 87, 197 (2016).
- [20] M. Birouk, N. Lekic, Liquid jet breakup in a quiescent atmosphere: a review, *Atomization and Sprays*, 19(6), 501 (2009).
- [21] R.D. Reitz, F.V. Bracco, Mechanisms of breakup of round liquid jets, in *Encyclopedia of Fluid Mechanics* (Gulf Publishing Co., 1986), Vol. 3, pp. 233-249.
- [22] S.P. Lin, R.D. Reitz, Drop and spray formation from a liquid jet, *Annu. Rev. Fluid Mech.*, 30, 85 (1998).
- [23] A. Erriguible, S. Vincent, P. Subra-Patternault, Numerical investigations of liquid jet breakup in pressurized carbon dioxide: Conditions of two-phase flow in Supercritical

- Antisolvent Process, *J. Supercrit. Fluids*, 63, 16 (2012).
- [24] A.H. Lefebvre, *Atomization and Sprays*, 1989, Hemisphere.
- [25] A. Loppinet-Serani, C. Aymonier, F. Cansell, Current and foreseeable applications of supercritical water for energy and the environment, *ChemSuschem*, 1(6), 486 (2008).
- [26] S. Marre, Y. Roig, C. Aymonier, Supercritical microfluidics: Opportunities in flow-through chemistry and materials science, *J. Supercrit. Fluids*, 66, 251 (2012).
- [27] S. Ogden, R. Boden, M. Do-Quang, Z. Wu, G. Amberg, K. Hjort, Fluid behavior of supercritical carbon dioxide with water in a double-Y-channel microfluidic chip, *Microfluidics and Nanofluidics*, 17(6), 1105 (2014).
- [28] N. Qin, J.Z. Wen, C.L. Ren, Highly pressurized partially miscible liquid-liquid flow in a micro-T-junction. I. Experimental observations, *Phys. Rev. E*, 95, 043110 (2017).
- [29] S. Marre, C. Aymonier, P. Subra, E. Mignard, Dripping to jetting transitions observed from supercritical fluid in liquid microflows, *Appl. Phys. Lett.*, 95, 134105 (2009).
- [30] See Supplemental Material at [URL will be inserted by publisher] for the Rayleigh breakup regime movie.
- [31] See Supplemental Material at [URL will be inserted by publisher] for the sinuous wave breakup regime movie.
- International Journal of Multiphase Flow 12(5), 745 (1986).
- [34] R. Guillaument, A. Erriguible, C. Aymonier, S. Marre, P. Subra-Paternault, Numerical simulation of dripping and jetting in supercritical fluids/liquid micro coflows, *J. Supercrit. Fluids*, 81, 15 (2013).
- [35] J.U. Brackbill, A continuum method for modeling surface tension, *Journal of Computational Physics* 100(2), 335-354 (1992).
- [36] D. L. Youngs, Time-dependent multi-material flow with large fluid distortion. In Morton, K. W., Baines, M. J., *Numerical Methods for Fluid Dynamics*, Academic Press, New-York (1982).
- [37] See Supplemental Material at [URL will be inserted by publisher] for (i) the 2D simulation of the atomization-like breakup regime including the velocity vectors and the pressure field and (ii) the 3D simulation of the same regime.
- [38] <https://www.nist.gov/srd/refprop>.
- [39] A. Hebach, A. Oberhof, N. Dahmen, A. Kogel, H. Ederer, E. Dinjus, Interfacial Tension at Elevated Pressures-Measurements and Correlations in the Water + Carbon Dioxide System, *J. Chem. Eng. Data*, 47, 1540 (2002).
- [40] A. Zandian, W.A. Sirignano, F. Hussain, Planar liquid jet: Early deformation and atomization cascades, *Phys. Fluids*, 29, 062109 (2017).
- [41] W.C. Jeong, J.M. Lim, J.H. Kim, Y.J. Lee, S.H. Kim, G. Lee, J.D. Kim, G.R. Yi, S.M. Yang, Controlled generation of submicron emulsion droplets via highly stable tip-streaming mode in microfluidic devices, *Lab Chip*, 12, 1446 (2012).
-
- * erriguible@enscbp.fr
- † <http://www.icmcb-bordeaux.cnrs.fr>;
Samuel.Marre@icmcb.cnrs.fr
- [33] I. Kataoka, Local instant formulation of two-phase flow,